



16 **Abstract**

17 The best occurrence of blueschist-facies lithologies in Himalaya is that of the Shergol Ophiolitic  
18 M $\acute{e}$ lange along the Indus suture zone in Ladakh region of north-western India. These lithologies  
19 are characterized by well preserved lawsonite-glaucophane-garnet-quartz assemblages. This  
20 paper presents for the first time the results of a detailed fluid inclusion study on these  
21 lithologies, in order to understand the fluid P-T evolution and its tectonic implications.

22 The blueschist rocks from Shergol Ophiolitic M $\acute{e}$ lange record metamorphic peak conditions at  
23  $\sim 19$  kbar,  $470^{\circ}\text{C}$ . Several types of fluid inclusions are trapped in quartz and garnet, most of  
24 them being two-phase at room temperature. Three types of fluid inclusions have been  
25 recognised, basing on microtextures and fluid composition: Type-I are primary two-phase  
26 carbonic-aqueous fluid inclusions ( $V_{\text{CO}_2} - L_{\text{H}_2\text{O}}$ ); Type-II are two-phase ( $L_{\text{H}_2\text{O}} - V_{\text{H}_2\text{O}}$ ) aqueous  
27 fluid inclusions, either primary (Type-IIa) or secondary (Type-IIb); Type-III are re-  
28 equilibrated fluid inclusions. In the Type-I primary carbonic-aqueous inclusions,  $\text{H}_2\text{O}$  is  
29 strongly predominant with respect to  $\text{CO}_2$ ; the homogenization temperature of  $\text{CO}_2$  range from  
30  $-7$  to  $-2^{\circ}\text{C}$ . The clathrate melting temperature in such inclusions varies in between  $+7.1$  to  
31  $+8.6^{\circ}\text{C}$ . Type-II two-phase aqueous fluid inclusions show a wide range of salinity, from  $7.8$ –  
32  $14$  wt.%  $\text{NaCl}_{\text{eq}}$  (Type-IIa) to  $1.65$ – $6.37$  wt.%  $\text{NaCl}_{\text{eq}}$  (Type-IIb) with accuracy  $\pm 0.4$ wt.%  
33  $\text{NaCl}_{\text{eq}}$ .

34 Type-I and Type-IIa primary fluid inclusions are hosted in peak minerals (garnet and quartz  
35 included in garnet), therefore they were likely entrapped at, or near to, peak P-T conditions.

36 The dominantly aqueous fluid of both Type-I and Type-IIa inclusions was most likely produced  
37 through metamorphic devolatilization reactions occurring in the subducting slab. Despite their  
38 primary nature, the isochores of Type-I and Type-IIa inclusions do not intersect the peak  
39 metamorphic conditions of the blueschist mineral assemblage, suggesting that these inclusions  
40 stretched or re-equilibrated during nearly isothermal decompression from  $19$  kbar to  $3$  kbar or

41 less, at  $T=290^{\circ}\text{C}$ . This conclusion is further supported by their large variability in shapes and  
42 sizes which range from irregular inclusions ('C'/arc shaped, hook shape and satellite type). This  
43 decompression stage was followed by nearly isobaric cooling, testified by the occurrence of  
44 dendritic networks of decrepitated and 'imploded' fluid inclusions.

45 Key Words: Fluid inclusions, Blueschist, lawsonite, Ladakh, Himalaya

46

## 47 **1. Introduction**

48 Fluid inclusions occurring in high pressure – low temperature (HP-LT) metamorphic rocks  
49 reveal the nature of fluid as well as the role of fluid in the subduction history of continental or  
50 oceanic crust. Fluid inclusions can also be used as a marker point in constraining parts of the  
51  $P$ – $T$  paths of different metamorphic rocks (e.g. Hollister et al., 1979; Santosh, 1987; Hames et  
52 al., 1989; Sisson et al., 1989; Vry and Brown, 1991; Winslow et al., 1994). Additionally,  
53 evidences of fluid–rock interactions occurred during blueschist- and eclogite- facies  
54 metamorphism can provide significant insights for our understanding of fluid storage and  
55 recycling during subduction or continent-continent collision processes (Brunnsman et al., 2000;  
56 Scambelluri and Phillipott, 2001).

57 The post-entrapment modification of the size and shape of fluid inclusions in response to  
58 deformation, cooling or decompression can help to constrain the  $P$ - $T$  paths of their host rocks  
59 and hence provide some insights on their exhumation processes (e.g. Scambelluri, 1992;  
60 Winslow et al., 1994, Vallis and Scambelluri, 1996; Kuster and Stockhert, 1997; El-Shazly and  
61 Sisson, 1999; Bakker and Mamtani, 2000). The detailed observation of the fluid inclusion  
62 textures and microthermometric results hold the key to fruitful data elucidation (e.g. Bodnar et  
63 al., 1989; Sterner and Bodnar, 1989; Vityk et al., 1994; 1995; Barker, 1995; Sterner et al., 1995;  
64 Vityk and Bodnar, 1995; Van den Kerkhof and Hein, 2001).

65 Fluid inclusion studies on subduction-related metamorphic rocks often revealed that the fluid  
66 was retained within the subducting slab and that the fluid flow was limited (e.g. El-Shazly and  
67 Sisson, 1999; Xiao et al., 2000; Gao and Klemnd, 2001). However, previous fluid inclusion  
68 studies focused on HP-LT metamorphic terranes show no general agreement on fluid  
69 composition and mechanisms of fluid flow.

70 Blueschists occur in many orogenic belts including the Pacific, Alpine-Himalayan and  
71 Precambrian-Phanerozoic belts (Liou et al., 1990). Most of the studies on the blueschist-facies  
72 rocks are focused on petrology, mineralogy and geochronology (e.g. Martin et al., 2011; Vitale  
73 Brovarone et al., 2011; Chantel et al., 2012; Abers et al., 2013; Cao et al., 2013; Kim et al.,  
74 2013; Spandler and Pirard, 2013), whereas the application of fluid inclusion studies to  
75 blueschist-facies rocks is limited so far to few examples. Luckscheiter and Morteani (1980)  
76 noticed the presence of CO<sub>2</sub>-H<sub>2</sub>O fluids in glaucophane-bearing rocks from the Tauern  
77 Window, while Barr (1990) reported the presence of only aqueous fluid in blueschist rocks  
78 from Syros. Invernizzi et al. (1996) studied the fluid inclusions in quartz veins hosted within  
79 blueschist-facies rocks, and inferred the re-equilibration history of these fluid inclusions in  
80 terms of uplift processes. The re-equilibration of the vast majority of primary fluid inclusions  
81 in high *P*-low *T* rocks during exhumation is the main cause for the scarcity of such studies  
82 (Touret, 1992). However, Vityk et al. (1994) and Vityk and Bodnar (1995) experimental works  
83 on synthetic fluid inclusions presented textural benchmarks for recreating sections of *P*-*T* paths  
84 and for enhancing tectonic interpretations.

85 Although the Himalaya is the archetype of collisional orogens, high-pressure metamorphic  
86 rocks are rare (e.g. Lombardo and Rolfo, 2000; Guillot et al., 2008). The blueschist-facies rocks  
87 in Himalaya are mostly lawsonite-bearing and occur along the Indus Suture Zone in Pakistan  
88 (Shangla: Shams, 1972; Frank et al., 1977) and NW India (Sapi–Shergol, Ladakh: Honegger et  
89 al., 1989; Groppo et al., 2016; Zildat: Viridi et al., 1977). Few lawsonite- and epidote blueschist-

90 facies rocks are also reported from the eastern portion of the orogen in the Indo-Burmese  
91 Ranges (Nagaland Ophiolite Complex: Ghose and Singh, 1980; Chatterjee and Ghose, 2010;  
92 Ao and Bhowmik, 2014). The preservation of lawsonite in the blueschists indicates very low  
93 geothermal gradients during subduction as well as during exhumation processes. The best  
94 occurrence of such lithologies in the Himalaya is that of Sapi-Shergol: a preliminary petrologic  
95 study of these blueschists by Honegger et al. (1989) constrained peak P-T conditions at 9-11  
96 kbar, 350-450°C (conventional thermobarometry). Groppo et al. (2016) estimated significantly  
97 higher pressure (19 kbar, 470°C) for the same unit by using *P-T* pseudosection modelling and  
98 suggested a very low geothermal gradient (i.e. 8-9°C/km). Sachan and Mukherjee (2001)  
99 preliminarily studied the fluids from quartz veins hosted in the blueschist rocks from Sapi-  
100 Shergol and provided comments upon their exhumation history. However, these quartz veins  
101 are related to a very late stage of the metamorphic evolution, and consequently do not give any  
102 direct clue on the blueschist formation and exhumation.

103 As concerning other subduction-related rocks from the Himalaya, a fluid inclusion study by  
104 Mukherjee and Sachan (2009) focusing on the ultra-high pressure eclogites from the Tso  
105 Morari, showed the prevalence of high-salinity brine, N<sub>2</sub>, CH<sub>4</sub>, CO<sub>2</sub> –bearing fluids and low-  
106 salinity aqueous fluids. This study shows the complex nature of the fluid involved during deep  
107 subduction and exhumation of Indian continental crust. Additionally, Ferrando et al. (2007)  
108 reported the presence of pure CO<sub>2</sub> and CO<sub>2</sub>-H<sub>2</sub>O fluids in granulitized eclogites from eastern  
109 Himalaya.

110 This paper is the first systematic fluid inclusion study on the blueschist rocks from Sapi-Shergol  
111 ophiolitic mélange (Ladakh Himalaya, NW India). The fluids associated to peak and retrograde  
112 metamorphic stages are characterised, and the source of these fluids is assessed. Moreover, the  
113 fluid evolution is discussed in relation to the P–T paths inferred by Groppo et al. (2016) on the  
114 base of thermodynamic modelling. The results from this study have important implications for

115 the understanding of the nature and role of fluids during subduction-related metamorphism and  
116 the consequent uplift, in the framework of the geodynamic evolution of the Himalayan orogeny.

117

## 118 **2. Geological Setting**

119 The blueschists studied in this paper occur along the Indus suture zone in Ladakh, NW India  
120 (Fig. 1a). From SE to NW, blueschist-facies lithologies are reported at Zildat, Urtsi, Hinju, and  
121 Sapi-Shergol (Honegger et al., 1989). Among these occurrences, the largest one is that of Sapi-  
122 Shergol in western Ladakh, south of Kargil. Tectonically, the Sapi–Shergol blueschists belong  
123 to a narrow belt and are part of an ophiolitic *mélange* (Honegger et al., 1989) (Fig. 1b).

124 This ophiolitic *mélange* is thrust over the Kargil Molasse to the west as well as to the north,  
125 and it is in contact with the Nindam and Lamayuru Formations to the north and to the south,  
126 respectively. To the south, the Triassic limestone of the Zaskar Unit is thrust over the  
127 *mélange* (Frank et al., 1977, Honegger et al., 1982). The ophiolitic *mélange* is inferred to be a  
128 remnant of a paleo-accretionary prism produced by the northward subduction of the Neo-  
129 Tethys, originally separating the Ladakh arc to the south from the Asian active margin to the  
130 north (Mahéo et al., 2006) (Fig.1a). This paleo-accretionary prism comprises sedimentary  
131 bodies including mainly basic lithologies that have been metamorphosed under low-grade to  
132 lawsonite blueschist-facies conditions (Frank et al., 1977; Honegger et al., 1989; Reuber et al.,  
133 1987; Ahmad et al., 1996; Rolfo et al., 1997; Robertson, 2000; Mahéo et al., 2006). The Sapi–  
134 Shergol ophiolitic *mélange* therefore shows a complex internal architecture, including a number  
135 of slivers of the paleo-accretionary prism, intercalated with numerous slivers of other units  
136 including the Nindam and Lamayuru Formations, as well as low-grade meta-ophiolitic rocks  
137 with serpentinitized peridotites intruded by basic dikes (“sheared serpentinites” of Robertson,  
138 2000).

139 The protoliths of the blueschist lithologies cropping out around the Shergol village are mainly  
140 basic metavolcanics and volcanoclastites with subordinate amounts of cherts, metasediments  
141 and minor carbonatic lithologies. Mahéo et al. (2006) suggested that the blueschists originate  
142 from calc-alkaline igneous rocks formed in an intra-oceanic arc environment. Whole-rock and  
143 glaucophane K–Ar geochronology gave an age of ca. 100 Ma for the high-pressure  
144 metamorphic peak (Honegger et al., 1989). Petrographically, metabasic rocks are mainly fine-  
145 grained glaucophane -bearing schists, with lawsonite and minor clinopyroxene and phengite.  
146 Metavolcanoclastic rocks show a clastic structure with irregular fragments of metabasic rocks  
147 set in a very fine-grained matrix. The clasts generally contain a blue amphibole + lawsonite ±  
148 clinopyroxene assemblage. The matrix is very fine-grained and mainly comprises blue  
149 amphibole, chlorite and minor aegirine.

150 Silicic and impure carbonatic metasediments are locally found as intercalations within the  
151 metabasic and metavolcanoclastic rocks. The silicic metasediments comprise glaucophane +  
152 lawsonite + phengite ± garnet schists, lawsonite + glaucophane + phengite + garnet quartzitic  
153 micaschists and glaucophane + garnet + phengite quartzites. Lawsonite and garnet are either  
154 fine-grained or porphyroblastic. Lawsonite and garnet porphyroblasts are from few centimeters  
155 to few millimeters in size, and generally overgrow the main foliation. The impure carbonatic  
156 metasediments are very fine-grained and mainly consist of lawsonite, calcite, glaucophane, and  
157 minor phengite ± prehnite.

158

### 159 **3. Petrography**

160 A detailed petrographic study of two representative samples of metasediments (samples 14-4B  
161 and 14-6F/G) has been carried out. These metapelites are mainly composed of lawsonite,  
162 glaucophane, garnet, phengite and quartz, with minor calcite concentrated in late veins.

163 Accessory minerals are titanite and pyrite. Both samples are very fresh, one of them being  
164 relatively fine-grained (sample 14-4B) compared to the other (sample 14-16F/G).

165 Sample 14-4B is characterised by alternating layers rich in quartz or lawsonite + glaucophane  
166 + phengite, respectively (Fig. 2a, b). Glaucophane occurs in both layers as fine-grained  
167 idioblasts; it shows characteristic zoning pattern with light blue core and a dark blue rim. The  
168 preferred orientation of glaucophane and phengite defines the main foliation. Garnet is weakly  
169 zoned and occurs as small idioblasts (Fig. 2b). Lawsonite occurs as fine-grained idioblasts (Fig.  
170 2c); it contains inclusions of quartz and titanite. In the quartz-rich layers, lawsonite locally  
171 shows a skeletal habit, being intergrown with quartz.

172 The main assemblage of sample 14-6F/G is lawsonite + glaucophane + phengite + garnet +  
173 quartz, with glaucophane occurring as a major constituent (Fig. 2d). Titanite occurs as accessory  
174 mineral. The main foliation, defined by the preferred orientation of glaucophane and minor  
175 phengite, is overgrown by lawsonite and garnet porphyroblasts and is locally crenulated (Fig.  
176 2d, e, f). The growth of lawsonite and garnet porphyroblasts pre-dated the crenulation event.  
177 Garnet occurs as medium- to coarse-grained idioblasts (Fig. 2e) locally included within the  
178 lawsonite porphyroblasts, and shows strong zoning. Variably sized inclusions of glaucophane,  
179 actinolite, phengite, quartz, chlorite and rare omphacite are found in garnet porphyroblasts.  
180 Glaucophane occurs as fine-grained nematoblasts in the matrix. Porphyroblastic lawsonite is  
181 up to 1 centimetre in size and sub-idioblastic, and overgrows the main foliation. Phengite is  
182 fine- to medium-grained and is found in association with glaucophane (Fig. 2d). The main  
183 foliation is locally crosscut by quartz  $\pm$  albite  $\pm$  chlorite veins (Fig. 2f). It is worth noting that  
184 in both samples, garnet was predicted to have grown at (or close to) peak P-T conditions, i.e. in  
185 the narrow P-T range of 400-470°C, 17-19 kbar (Groppo et al., 2016).

186

#### 187 4. Methods



188 Double polished wafers with a thickness of about  $0.4 \pm 0.2$  mm were prepared from the samples  
189 described in chapter 3. A microthermometric study was conducted on a Linkam THMSG 600  
190 stage mounted on Olympus microscope at the Wadia Institute Fluid inclusion Laboratory. The  
191 equations of Zhang and Frantz (1987) and Brown and Lamb (1989) were used for the estimation  
192 of isochores of aqueous fluid inclusions, whereas the equation of Bower and Helgeson (1985)  
193 was used for the calculation of isochores of  $\text{CO}_2$ – $\text{H}_2\text{O}$  inclusions in the “Flinco” computer  
194 program of Brown (1989).

195

## 196 **5. Fluid inclusion petrography**

197 We have studied fluid inclusions hosted in garnet and in matrix quartz, as well as in quartz  
198 included in garnet porphyroblasts belonging to the peak metamorphic mineral assemblage (i.e.  
199 garnet + lawsonite + glaucophane + phengite + quartz  $\pm$  omphacite; see Groppo et al., 2016).  
200 Texturally, two types of fluid inclusions have been found: regular shaped inclusions (Type-I  
201 and Type-II) and re-equilibrated inclusions (Type-III). Regular shaped inclusions are either  
202 two-phase carbonic-aqueous (Type-I) or two-phase aqueous (Type-II) inclusions. Type-II  
203 inclusions are more abundant than Type-I inclusions.

204 Type-I inclusions are two-phase inclusions ( $V_{\text{CO}_2} + L_{\text{H}_2\text{O}}$ ) at room temperature ( $\sim 27^\circ\text{C}$ ) and  
205 contain an aqueous-carbonic fluid (Fig. 3A, B). The size of these inclusions are small (average  
206 of  $9 \mu\text{m}$ ). The  $\text{CO}_2$  vapour has a variable volume proportion ranging from 10 to 30% of the total  
207 volume of the inclusion. These inclusions are systematically found as isolated occurrences  
208 within garnet and quartz, and are dispersed randomly in the host grains (Fig. 3A, B), therefore  
209 they have been interpreted as primary in origin; moreover, because garnet is a peak phase, Type-  
210 I inclusions have been entrapped at peak P-T conditions.

211 Type-II inclusions are two-phase aqueous ( $V_{\text{H}_2\text{O}} + L_{\text{H}_2\text{O}}$ ) inclusions and are further classified as  
212 Type-IIa and Type-IIb on the basis of their mode of occurrence. The size of these types of

213 inclusion ranges between 9 and 15  $\mu\text{m}$ . Type-IIa inclusions are isolated and randomly  
214 distributed in the matrix quartz as well as in quartz included in garnet grains, and are therefore  
215 interpreted as primary inclusions; they were likely entrapped at, or near to, peak P-T conditions  
216 because quartz included in garnet is a prograde-to-peak phase. Type-IIb are concentrated along  
217 microfractures of the host minerals and are interpreted as secondary inclusions. The trails of the  
218 secondary inclusions often cross-cut the grain margins (i.e. transgranular inclusions) (Fig. 3C,  
219 D).

220 Type-III inclusions are re-equilibrated inclusions showing partially dendritic type network as  
221 well as necking phenomena (Fig. 4A-D). The dendritic type network may be originated by the  
222 dissolution of inclusion walls, as well as by the closing of inclusion voids which lead to form  
223 numerous tails and channels filled by fluids (Invernizzi et al., 1998). Some inclusions show  
224 necking phenomena, and few also show “C” type microstructures. Some solitary inclusions  
225 surrounded by minute satellite inclusions are observed in matrix quartz.

226

## 227 **6. Microthermometric results**

228 Microthermometry reveals compositional variations of the fluid inclusions from aqueous-  
229 carbonic to aqueous. The results of microthermometric measurements are shown in histograms  
230 (Figs.5, 6 and 7) and summarized in Table 1. The Type-I aqueous-carbonic fluid inclusions  
231 hosted in the matrix quartz as well as in quartz included in garnet and in garnet itself, show  
232 initial melting temperature ( $T_{im}$ ) between  $-56.9^{\circ}\text{C}$  and  $-56.6^{\circ}\text{C}$ , thus suggesting a nearly pure  
233  $\text{CO}_2$  composition for the vapour phase. The homogenization temperature of  $\text{CO}_2$  in these  
234 inclusions lies between  $-7$  to  $-2^{\circ}\text{C}$  (Fig. 5B). The clathrate melting temperature was also  
235 observed in some carbonic-aqueous inclusions, which occurred between  $+7.1$  to  $8.6^{\circ}\text{C}$ . The  
236 total homogenization of such inclusions took place in between  $227^{\circ}$  and  $265^{\circ}\text{C}$  (Fig. 5A).

237 The Type-II two-phase aqueous inclusions mainly occur in matrix quartz as well as in quartz  
238 included in garnet. Type-IIa primary inclusions and Type-IIb secondary inclusions show  
239 different initial melting temperature ( $T_{im}$ ) and final melting temperature ( $T_{fm}$ ) values. Type  
240 IIa primary  $H_2O$ -NaCl inclusions show  $T_{im}$  in the range  $-21.2^\circ C$  to  $-22.6^\circ C$ ,  $T_{fm}$  of  $-5^\circ C$  to  
241  $-10^\circ C$  (Fig. 6A) and temperature of homogenization ( $T_h$ ) between  $250^\circ C$  and  $300^\circ C$  (Fig. 7B).  
242 The corresponding salinity ranges are estimated at 7.8–13.98 wt% NaCl equivalent, with  
243 density of  $0.863$ – $0.874$   $g/cm^3$ . Type-IIb secondary two-phase aqueous inclusions occurring in  
244 transgranular trails show a wider range of  $T_{im}$  ( $-21^\circ$  to  $-23^\circ C$ ), and significantly different  $T_{fm}$   
245 ( $-1^\circ$  to  $-4^\circ C$ ; Fig. 6 B) and  $T_h$  ( $145^\circ$  to  $220^\circ C$ ; Fig. 7A) values. The corresponding salinity  
246 ranges are estimated at 1.65–6.37 wt% NaCl equivalent, and density is in the range of  $0.889$ –  
247  $0.938$   $g/cm^3$ .

248 Composition and density of the fluid phase observed in the different generations of inclusions  
249 are used to calculate the isochores in the  $P$ – $T$  space, and the implications are discussed in a later  
250 section. The minimum  $T_h$  and the maximum  $T_h$  obtained from the peak value in Figs. 5,6,7 for  
251 each inclusion type were considered for construction of isochores, following the criteria given  
252 by Touret (2001),.

253

## 254 **7. Discussion**

255 The study of fluid inclusions provides important constraints on their trapping conditions  
256 (textural evidence in relation to  $P$ – $T$  estimates), composition and behaviour of metamorphic  
257 fluids. This is the first systematic fluid inclusion study on the blueschists from the Sapi-Shergol  
258 ophiolitic mélange that correlates  $P$ - $T$  data from mineral geothermobarometry and fluid  
259 inclusions. Our results reveal the pervasive presence of aqueous-carbonic and aqueous fluids  
260 preserved in quartz and garnet.

261

## 262        *7.1. Interpretation of fluid inclusions textures*

263        In the studied samples, the isolated nature of Type-I aqueous-carbonic inclusions and of Type-  
264        IIa two-phase aqueous inclusions hosted in quartz and garnet reveals that they may have formed  
265        during the crystallization of their host minerals, and may thus be considered to be trapped early  
266        during the mineral growth (Roedder, 1984). Moreover, because garnet is a peak phase, the  
267        primary Type-I and Type-IIa inclusions have been entrapped at, or near to, peak P-T conditions.  
268        Type-IIb two-phase aqueous inclusions occur in transgranular trails and are therefore clearly  
269        secondary in nature.

270        Concerning Type-III inclusions, the most commonly observed features are: (i) necking, (ii)  
271        inclusions with 'C' or Arc shaped microstructure, (iii) satellite inclusions, (iv) hook shaped or  
272        annular inclusions, (v) dendritic network of inclusions (Fig.4 A, B, C & D). The necking  
273        textures are interpreted as related to intense dissolution of the inclusion walls to produce highly  
274        irregular inclusion morphology. These microtextures were likely formed along a decompression  
275        path: fractures initially developed along the inclusion planes in which inclusions primarily  
276        necked down, and later on they were stretched (Fig 4C). The inclusions displaying a hook-like  
277        morphology or annular textures (Fig.4C) are similar to inclusions formed under isothermal  
278        decompression (ITD), as shown in the experimental work of Sterner and Bodnar (1989), Vityk  
279        and Bodnar (1995), and Bodnar (2003). Boullier et al. (1991) proposed that annular textures are  
280        symptomatic of an anisotropic stress environment. Satellite inclusions around a bigger solitary  
281        inclusion are analogous to 'explosion' textures described for natural and synthetic fluid  
282        inclusions in quartz that have experienced overpressures caused by 'near isothermal  
283        decompression' (e.g., Bodnar et al., 1989; Vityk et al., 1994; Vityk and Bodnar, 1995). Opposite  
284        to these microtextures which are related to decompression, the development of dendritic  
285        networks of imploded inclusions in quartz is indicative of near isobaric cooling (IBC) in the  
286        last stages of metamorphic evolution. This type of texture is similar to that described by Vityk

287 et al. (1994) and Vityk and Bodnar (1995) for their experimental work during isobaric cooling  
288 (IBC).

289

## 290 **7.2. *Nature and Source of Fluids***

291 Two types of fluid (aqueous-carbonic and aqueous) have been found in the blueschist mineral  
292 assemblage. Type-I aqueous-carbonic fluids occur as primary inclusions in peak metamorphic  
293 garnet as well as in quartz. Type-IIa aqueous fluid with high saline nature is preserved as  
294 primary inclusions in matrix quartz, as well as in quartz included in garnet, whereas Type-IIb  
295 aqueous fluid with low saline nature is observed as secondary inclusions in quartz.

296 Type-I aqueous-carbonic inclusions have constant vapour: liquid ratios (i.e. 30:70). The  
297 temperature of clathrate melting and the homogenization temperature of the CO<sub>2</sub> phase in these  
298 inclusions indicate that they are predominantly aqueous with a small amount of CO<sub>2</sub>,  
299 consistently with the stability of lawsonite at peak metamorphic conditions. According to  
300 Groppo et al. (2016), in fact, the contemporaneous growth of lawsonite and garnet would have  
301 been enhanced by a protracted H<sub>2</sub>O influx at the relatively high pressure of ca. 17–18 kbar. The  
302 predominance of aqueous fluids in high P metamorphic assemblages is also shown in previous  
303 studies which call upon substantial fluid release at high P–T conditions (e.g. Clarke et al., 2006;  
304 Tsujimori and Ernst, 2014; Ulmer and Trommsdorff, 1995; Scambelluri et al., 2004; Poli and  
305 Schmidt, 1995; Poli et al., 2009) through metamorphic devolatilization reactions occurring in  
306 the subducting slab (Bebout, 1991, 1995; Jarrard, 2003).

307

## 308 **7.3. *Reconstruction of the P-T-fluid history***

309 P–T estimates based on conventional thermobarometry proposed peak conditions of 350–420  
310 °C, 9–11 kbar for the Sapi-Shergol blueschists (Honegger et al., 1989). Petrologic modeling  
311 performed by our research team (Groppo et al., 2016) inferred peak P–T conditions significantly

312 higher than those previously estimated, i.e. ca. 470 °C, 19 kbar. According to Groppo et al.  
313 (2016), the estimated peak metamorphic conditions suggest that the blueschists experienced a  
314 cold subduction history along a very low to low thermal gradient (“early” prograde: ca. 5–6  
315 °C/km; “late” prograde: ca. 7–8 °C/km). The preservation of lawsonite in the studied lithologies  
316 further indicate that the exhumation process must have been coupled with substantial cooling  
317 (i.e. without crossing the lawsonite-out boundary; Zack et al., 2004).

318 As concerning the fluid evolution, isochores are plotted in comparison with the  $P$ – $T$  path  
319 inferred on the basis of thermodynamic modelling and thermobarometry (Fig. 8). Isochores of  
320 both Type-I aqueous–carbonic inclusions and Type-II aqueous inclusions plot in the lower part  
321 of the  $P$ – $T$  space. Although these inclusions are texturally primary and are hosted within peak  
322 minerals (garnet and quartz included in garnet), they do not plot along the prograde  $P$ – $T$  path  
323 or at peak metamorphic conditions, thus suggesting that these inclusions must have experienced  
324 considerable leakage and re-equilibration, resulting in only low-density fluid eventually  
325 preserved in the inclusions. Therefore, it is assumed that Type-I  $\text{CO}_2$ – $\text{H}_2\text{O}$  and Type-IIa aqueous  
326 inclusions most likely formed at or near the peak  $P$ – $T$  conditions at ~ 19 kbar, ~ 450°C, but  
327 they were later re-equilibrated during exhumation. The isochores of secondary aqueous  
328 inclusions (Type IIa) plots above the isochores of primary inclusions because the secondary  
329 aqueous inclusions originate at lower temperature and their densities are thus higher (Fig.8).

330 Evidences of such a pervasive re-equilibration are very clearly represented by the textural  
331 features of Type-III fluid inclusions described in the previous chapters (Fig.4). The observed  
332 textural features are indicative either of re-equilibration occurred during isothermal  
333 decompression, as well as during isobaric cooling at the final stages of exhumation. Similar  
334 high degrees of re-equilibration of fluid inclusions during retrogression is well documented by  
335 Sterner and Bodnar (1989) and Kuster and Stockhert (1997) for high- $P$  and low- $T$  rocks. We  
336 therefore suggest that these re-equilibrated inclusions might have been trapped during the early

337 stages of subduction, while their re-equilibration took place during the subsequent fast  
338 exhumation. Such high internal underpressure at low temperature would develop only when the  
339 subduction / burial path is very steep and consequently follows very low geothermal gradients;  
340 the preservation of lawsonite in the studied blueschist facies lithologies strongly support the  
341 scenario in which very low geothermal gradients were prevailing during initial subduction as  
342 well as during exhumation (Fig. 8). The presence of dendritic network type inclusions suggests  
343 isobaric cooling (as evidenced by the experimental studies of Bodnar et al., 1989; Vityk et al.,  
344 1994; Vityk and Bodnar, 1995). The hook like inclusions were likely trapped at about 3 kbar  
345 (Vityk and Bodnar, 1995), whereas the implosion texture formed at higher pressure (Boulier,  
346 1999). In our case, the last stage of the P-T evolution is represented by the isobaric cooling after  
347 the isothermal decompression, therefore we suggest that the dendritic morphology might have  
348 been formed at this last stage (Fig. 8). This interpretation is clearly compatible with the broad  
349 geological setting of the area.

350

## 351 **8. Conclusions**

352 The first detailed fluid inclusions study of Himalayan blueschist-facies lithologies from the  
353 Sapi-Shergol ophiolitic mélangé in the Indus suture zone, revealed predominantly CO<sub>2</sub>-H<sub>2</sub>O  
354 and H<sub>2</sub>O-NaCl inclusions. The primary CO<sub>2</sub>-H<sub>2</sub>O and H<sub>2</sub>O-NaCl inclusions were trapped by  
355 host minerals at peak P-T conditions. The fluid was most likely produced through metamorphic  
356 devolatilization reactions occurring in the subducting slab. Additional multiple generations of  
357 re-equilibrated inclusions show characteristic morphologies developed in response to fast rates  
358 of uplift. A nearly isothermal decompression path followed peak metamorphic P-T condition  
359 and is characterized by stretching, necking and formation of “C” or hook-like shaped inclusions.  
360 A veining stage is associated to late isobaric cooling and is characterized by the local  
361 development of a dendritic network of fluid inclusions.

362

363 **Acknowledgments**

364 HKS, AK, PCS and ST are thankful to the Director of the Wadia Institute of Himalayan  
365 Geology, Dehradun, for providing lab facilities and encouragement to carry out this work. An  
366 nonymous reviewer and the journal editor provided useful suggestions, which led to significant  
367 improvement of the manuscript. This study is part of a Cooperation Agreement between the  
368 Wadia Institute of Himalayan Geology (Dehradun, India) and the University of Torino, Dept.  
369 of Earth Sciences (Torino, Italy). Fieldwork of FR and CG was supported by University of  
370 Torino—Call 1—Junior PI Grant (TO\_Call1\_2012\_0068).



371 **References**

- 372 Abers, G. A., Nakajima, J., van Keken, P. E., Kita, S., Hacker, B. R., 2013. Thermal–  
373 petrological controls on the location of earthquakes within subducting plates. *Earth and*  
374 *Planetary Science Letters* 369, 178-187.
- 375 Ahmad, T., Islam, R., Khanna, P. P., Thakur, V. C., 1996. Geochemistry, petrogenesis and  
376 tectonic significance of the basic volcanic units of the Zildat ophiolitic mélange, Indus suture  
377 zone, eastern Ladakh (India). *Geodinamica Acta* 9, 222-233.
- 378 Ao, A., Bhowmik, S. K., 2014. Cold subduction of the Neotethys: the metamorphic record from  
379 finely banded lawsonite and epidote blueschists and associated metabasalts of the Nagaland  
380 Ophiolite Complex, India. *Journal of Metamorphic Geology* 32, 829-860.
- 381 Bakker, R. J., Mamtani, M. A., 2000. Fluid inclusions as metamorphic process indicators in the  
382 Southern Aravalli Mountain Belt (India). *Contributions to Mineralogy and Petrology* 139, 163-  
383 179.
- 384 Barker, A. J., 1995. Post-entrapment modification of fluid inclusions due to overpressure:  
385 evidence from natural samples. *Journal of Metamorphic Geology* 13, 737-750.
- 386 Barr, H., 1990. Preliminary fluid inclusion studies in a high-grade blueschist terrain, Syros,  
387 Greece. *Mineralogical Magazine* 54, 159-168.
- 388 Bebout, G. E., 1991. Field-based evidence for devolatilization in subduction zones:  
389 Implications for arc magmatism. *Science* 251, 413-416.
- 390 Bebout, G. E., 1995. The impact of subduction-zone metamorphism on mantle-ocean chemical  
391 cycling. *Chemical Geology* 126, 191-218.
- 392 Bodnar, R. J., 2003. Reequilibration of fluid inclusions. *Fluid inclusions: Analysis and*  
393 *interpretation* 32, 213-230.

394 Bodnar, R. J., Binns, P. R., Hall, D. L., 1989. Synthetic fluid inclusions-VI. Quantitative  
395 evaluation of the decrepitation behaviour of fluid inclusions in quartz at one atmosphere  
396 confining pressure. *Journal of Metamorphic Geology* 7, 229-242.

397 Boullier, A. M., France-Lanord, C., Dubessy, J., Adamy, J., Champenois, M., 1991. Linked  
398 fluid and tectonic evolution in the High Himalaya mountains (Nepal). *Contributions to*  
399 *Mineralogy and Petrology* 107, 358-372.

400 Bowers, T. S., Helgeson, H. C., 1983. Calculation of the thermodynamic and geochemical  
401 consequences of nonideal mixing in the system  $H_2O-CO_2-NaCl$  on phase relations in geologic  
402 systems: Equation of state for  $H_2O-CO_2-NaCl$  fluids at high pressures and temperatures.  
403 *Geochimica et Cosmochimica Acta* 47, 1247-1275.

404 Brovarone, A. V., Groppo, C., Hetényi, G., Compagnoni, R., Malavieille, J., 2011. Coexistence  
405 of lawsonite-bearing eclogite and blueschist: phase equilibria modelling of Alpine Corsica  
406 metabasalts and petrological evolution of subducting slabs. *Journal of Metamorphic Geology*  
407 29, 583-600.

408 Brown, P. E., 1989. FLINCOR; a microcomputer program for the reduction and investigation  
409 of fluid-inclusion data. *American Mineralogist* 74, 1390-1393.

410 Brown, P. E., Lamb, W. M., 1989. P-V-T properties of fluids in the system  $H_2O \pm CO_2 \pm NaCl$ :  
411 New graphical presentations and implications for fluid inclusion studies. *Geochimica et*  
412 *Cosmochimica Acta* 53, 1209-1221.

413 Cao, Y., Jung, H., Song, S., 2013. Petro-fabrics and seismic properties of blueschist and eclogite  
414 in the North Qilian suture zone, NW China: Implications for the low-velocity upper layer in  
415 subducting slab, trench-parallel seismic anisotropy, and eclogite detectability in the subduction  
416 zone. *Journal of Geophysical Research: Solid Earth* 118, 3037-3058.

417 Chantel, J., Mookherjee, M., Frost, D. J., 2012. The elasticity of lawsonite at high pressure and  
418 the origin of low velocity layers in subduction zones. *Earth and Planetary Science Letters* 349,  
419 116-125.

420 Chatterjee, N., Ghose, N. C., 2010. Metamorphic evolution of the Naga Hills eclogite and  
421 blueschist, Northeast India: implications for early subduction of the Indian plate under the  
422 Burma microplate. *Journal of Metamorphic Geology* 28, 209-225.

423 Clarke, G. L., Powell, R., Fitzherbert, J. A., 2006. The lawsonite paradox: a comparison of field  
424 evidence and mineral equilibria modelling. *Journal of Metamorphic Geology* 24, 715-725.

425 El-Shazly, A. K., Sisson, V. B., 1999. Retrograde evolution of eclogite facies rocks from NE  
426 Oman: evidence from fluid inclusions and petrological data. *Chemical Geology* 154, 193-223.

427 Ferrando, S., Rolfo, F., Lombardo, B., 2007. Fluid evolution from metamorphic peak to  
428 exhumation in Himalayan granulitised eclogites, Ama Drime range, southern Tibet. *Eur. J.*  
429 *Mineral.* 19, 439–461.

430 Frank, W., Gansser, A., Trommsdorff, V., 1977. Geological observations in the Ladakh area  
431 (Himalayas): a preliminary report. *Schweiz. mineral. petrogr. Mitt* 57, 89-113.

432 Gao, J., Klemd, R., 2001. Primary fluids entrapped at blueschist to eclogite transition: evidence  
433 from the Tianshan meta-subduction complex in northwestern China. *Contributions to*  
434 *Mineralogy and Petrology* 142, 1-14.

435 Ghose, N. C., Singh, M. R., 1980. Occurrence of blueschist facies in the ophiolite belt of Naga  
436 Hills, east of Kiphire, NE India. *Geologische Rundschau* 69, 41-48.

437 Giaramita, M. J., Sorensen, S. S., 1994. Primary fluids in low-temperature eclogites: evidence  
438 from two subduction complexes (Dominican Republic, and California, USA). *Contributions to*  
439 *Mineralogy and Petrology* 117, 279-292.

440 Groppo, C., Rolfo, F., Sachan, H. K., Rai, S. K., 2016. Petrology of blueschist from the Western  
441 Himalaya (Ladakh, NW India): Exploring the complex behavior of a lawsonite-bearing system  
442 in a paleo-accretionary setting. *Lithos* 252, 41-56.

443 Guillot, S., Mahéo, G., de Sigoyer, J., Hattori, K.H. Pecher, A., 2008. Tethyan and Indian  
444 subduction viewed from the Himalayan high- to ultrahigh-pressure metamorphic rocks.  
445 *Tectonophysics* 451, 225–241.

446 Hames, W. E., Tracy, R. J., Bodnar, R. J., 1989. Postmetamorphic unroofing history deduced  
447 from petrology, fluid inclusions, thermochronometry, and thermal modeling: An example from  
448 southwestern New England. *Geology* 17, 727-730.

449 Hollister, L. S., Burruss, R. C., Henry, D. L., Hendel, E. M., 1979. Physical conditions during  
450 uplift of metamorphic terranes, as recorded by fluid inclusions. *Bulletin de Mineralogie* 102,  
451 555-561.

452 Honegger, K., Le Fort, P., Mascle, G., Zimmermann, J. L., 1989. The blueschists along the  
453 Indus suture zone in Ladakh, NW Himalaya. *Journal of Metamorphic Geology* 7, 57-72.

454 Invernizzi, C., Vityk, M., Cello, G., Bodnar, R., 1998. Fluid inclusions in high pressure/low  
455 temperature rocks from the Calabrian Arc (Southern Italy): the burial and exhumation history  
456 of the subduction-related Diamante-Terranova unit. *Journal of Metamorphic Geology* 16, 247-  
457 258.

458 Jarrard, R. D., 2003. Subduction fluxes of water, carbon dioxide, chlorine, and potassium.  
459 *Geochemistry, Geophysics, Geosystems*, 4(5).

460 Kim, D., Katayama, I., Michibayashi, K., Tsujimori, T., 2013. Deformation fabrics of natural  
461 blueschists and implications for seismic anisotropy in subducting oceanic crust. *Physics of the*  
462 *Earth and Planetary Interiors* 222, 8-21.

463 Klemm, R., 1989. PT evolution and fluid inclusion characteristics of retrograded eclogites,  
464 Münchberg Gneiss Complex, Germany. *Contributions to Mineralogy and Petrology* 102, 221-  
465 229.

466 Klemm, R., Van den Kerkhof, A. M., Horn, E. E., 1992. High-density CO<sub>2</sub> – N<sub>2</sub> inclusions in  
467 eclogite-facies metasediments of the Münchberg gneiss complex, SE Germany. *Contributions*  
468 *to Mineralogy and Petrology* 111, 409-419.

469 Küster, M., Stöckhert, B., 1997. Density changes of fluid inclusions in high-pressure low-  
470 temperature metamorphic rocks from Crete: a thermobarometric approach based on the creep  
471 strength of the host minerals. *Lithos* 41, 151-167.

472 Lombardo, B. Rolfo, F., 2000. Two contrasting eclogite types in the Himalayas: implications  
473 for the Himalayan orogeny. *Journal of Geodynamics* 30, 37–60.

474 Luckscheiter, B., Morteani, G., 1980. Microthermometrical and chemical studies of fluid  
475 inclusions in minerals from Alpine veins from the penninic rocks of the central and western  
476 Tauern Window (Austria/Italy). *Lithos* 13, 61-77.

477 Mahéo, G., Fayoux, C., Guillot, S., Garzanti, E., Capiez, P., Mascle, G., 2006. Geochemistry  
478 of ophiolitic rocks and blueschists from the Sapi-Shergol mélange (Ladakh, NW Himalaya,  
479 India): implication for the timing of the closure of the Neo-Tethys ocean. *Journal of Asian Earth*  
480 *Sciences* 26, 695-707.

481 Martin, L. A., Wood, B. J., Turner, S., Rushmer, T., 2011. Experimental measurements of trace  
482 element partitioning between lawsonite, zoisite and fluid and their implication for the  
483 composition of arc magmas. *Journal of Petrology*, egr018.

484 Mukherjee, B. K., Sachan, H. K., 2009. Behavior of fluids in coesite bearing rocks of Tso-  
485 Morari region, NW Himalaya: Implication for exhumation process. *Geological Magazine* 146,  
486 876-889.

487 Poli, S., Schmidt, M. W., 1995. H<sub>2</sub>O transport and release in subduction zones: experimental  
488 constraints on basaltic and andesitic systems. *Journal of Geophysical Research: Solid Earth*  
489 100(B11), 22299-22314.

490 Poli, S., Franzolin, E., Fumagalli, P., Crottini, A., 2009. The transport of carbon and hydrogen  
491 in subducted oceanic crust: an experimental study to 5 GPa. *Earth and Planetary Science Letters*  
492 278, 350-360.

493 Reuber, I., Colchen, M., Mevel, C., 1987. The geodynamic evolution of the South-Tethyan,  
494 margin in Zaskar, NW-Himalaya, as revealed by the Spongtag ophiolitic mélanges.  
495 *Geodinamica Acta* 1, 283-296.

496 Robertson, A. H. F., 2000. Formation of mélanges in the Indus suture zone, Ladakh Himalaya  
497 by successive subduction-related, collisional and post-collisional processes during late  
498 Mesozoic-late Tertiary time. *Geological Society, London, Special Publications* 170, 333-374.

499 Roedder, E., 1984. *Fluid Inclusions (Reviews in Mineralogy, Vol. 12)* Mineralogical Society  
500 of America. Washington, DC.

501 Rolfo, F., Lombardo, B., Compagnoni, R., Le Fort, P., Lemennicier, Y., Pêcher, A., 1997.  
502 *Geology and Metamorphism of the Ladakh Terrane and Shyok Suture Zone in the Chogo*  
503 *Lungma - Turmik area (northern Pakistan)*. *Geodinamica Acta* 10, 251-270.

504 Sachan, H. K., Mukherjee, B. K., 2001. Evidences of fluid re-equilibration in blueschist rocks  
505 from Shergol Ophiolitic Mélange, Indus Suture Zone, Ladakh. *Himalayan Geology* 22, 127-  
506 133.

507 Santosh, M., 1987. Cordierite gneisses of southern Kerala, India: petrology, fluid inclusions  
508 and implications for crustal uplift history. *Contributions to Mineralogy and Petrology* 96, 343-  
509 356.

510 Scambelluri, M., 1992. Retrograde fluid inclusions in eclogitic metagabbros from the Ligurian  
511 Western Alps. *European journal of mineralogy* 4, 1097-1112.

512 Scambelluri, M., Philippot, P., 2001. Deep fluids in subduction zones. *Lithos* 55, 213-227.

513 Scambelluri, M., Müntener, O., Ottolini, L., Pettke, T. T., Vannucci, R., 2004. The fate of B,  
514 Cl and Li in the subducted oceanic mantle and in the antigorite breakdown fluids. *Earth and*  
515 *Planetary Science Letters* 222, 217-234.

516 Selverstone, J., Spear, F.S., 1985. Metamorphic P–T Paths from pelitic schists and greenstones  
517 from the south-west Tauern Window, Eastern Alps. *Journal of metamorphic Geology* 3, 439-  
518 465.

519 Shams, F. A., 1972. Glaucofane-bearing rocks from near Topsin, Swat. First record from  
520 Pakistan. *Pakistan Journal of Scientific Research* 24, 343-345.

521 Sisson, V. B., Hollister, L. S., Onstott, T. C., 1989. Petrologic and age constraints on the origin  
522 of a low-pressure/high-temperature metamorphic complex, southern Alaska. *Journal of*  
523 *Geophysical Research: Solid Earth* 94(B4), 4392-4410.

524 Spandler, C., Pirard, C., 2013. Element recycling from subducting slabs to arc crust: A review.  
525 *Lithos* 170, 208-223.

526 Sterner, S. M., Bodnar, R. J., 1989. Synthetic fluid inclusions-VII. Re-equilibration of fluid  
527 inclusions in quartz during laboratory-simulated metamorphic burial and uplift. *Journal of*  
528 *Metamorphic Geology* 7, 243-260.

529 Sterner, S. M., Hall, D. L., Keppler, H., 1995. Compositional re-equilibration of fluid inclusions  
530 in quartz. *Contributions to Mineralogy and Petrology* 119, 1-15.

531 Thakur, V., Misra, D., 1984. Tectonic framework of the Indus and Shyok suture zones in eastern  
532 Ladakh, northwest Himalaya. *Tectonophysics* 101, 207-220.

533 Touret, J. L., 2001. Fluids in metamorphic rocks. *Lithos* 55, 1-25.

534 Touret, J., Van Hinte, J. E., 1992. Le rôle des fluides dans les zones de subduction: un séminaire  
535 du Collège de France aux Pays-Bas. *Proceedings of the Koninklijke Nederlandse Akademie*  
536 *van Wetenschappen* 95, 293-296.

537 Tsujimori, T., Ernst, W. G., 2014. Lawsonite blueschists and lawsonite eclogites as proxies for  
538 palaeo-subduction zone processes: a review. *Journal of Metamorphic Geology* 32, 437-454.

539 Ulmer, P., Trommsdorff, V., 1995. Serpentine stability to mantle depths and subduction-related  
540 magmatism. *Science* 268(5212), 858.

541 Vallis, F., Scambelluri, M., 1996. Redistribution of high-pressure fluids during retrograde  
542 metamorphism of eclogite-facies rocks (Voltri Massif, Italian Western Alps). *Lithos* 39, 81-92.

543 Van den Kerkhof, A. M., Hein, U. F., 2001. Fluid inclusion petrography. *Lithos* 55, 27-47.

544 Viridi, N. S., Thakur, V. C., Kumar, S., 1977. Blueschist facies metamorphism from the Indus  
545 suture zone of Ladakh and its significance. *Himalayan Geology* 7, 479-482.

546 Vityk, M. O., Bodnar, R. J., 1995. Textural evolution of synthetic fluid inclusions in quartz  
547 during reequilibration, with applications to tectonic reconstruction. *Contributions to*  
548 *Mineralogy and Petrology* 121, 309-323.

549 Vityk, M. O., Bodnar, R. J., Schmidt, C. S., 1994. Fluid inclusions as tectonothermobarometers:  
550 Relation between pressure-temperature history and reequilibration morphology during crustal  
551 thickening. *Geology* 22, 731-734.

552 Vry, J. K., Brown, P. E., 1991. Texturally-early fluid inclusions in garnets: evidence of the  
553 prograde metamorphic path? *Contributions to Mineralogy and Petrology* 108, 271-282.

554 Winslow, D. M., Bodnar, R. J., Tracy, R. J., 1994. Fluid inclusion evidence for an anticlockwise  
555 metamorphic P-T path in central Massachusetts. *Journal of Metamorphic Geology* 12, 361-371.

556 Xiao, Y., Hoefs, J., van den Kerkhof, A. M., Fiebig, J., Zheng, Y., 2000. Fluid history of UHP  
557 metamorphism in Dabie Shan, China: a fluid inclusion and oxygen isotope study on the coesite-  
558 bearing eclogite from Bixiling. *Contributions to Mineralogy and Petrology* 139, 1-16.

559 Zack, T., Rivers, T., Brumm, R., Kronz, A., 2004. Cold subduction of oceanic crust:  
560 implications from a lawsonite eclogite from the Dominican Republic. *European Journal of*  
561 *Mineralogy* 16, 909-916.



562 Zhang, Y. G., Frantz, J. D., 1987. Determination of the homogenization temperatures and  
563 densities of supercritical fluids in the system NaCl-KCl-CaCl<sub>2</sub>-H<sub>2</sub>O using synthetic fluid  
564 inclusions. *Chemical Geology* 64, 335-350.

565 **Figure Captions**

566 **Figure 1.** (A) Regional Geological Map of Ladakh Himalaya (adopted from Thakur and  
567 Misra, 1984, and Mahéo et al., 2006); (B) Geological map of Shergol ophiolitic mélange  
568 (after Honegger et al., 1989).

569

570 **Figure 2.** Representative microstructures of the studied blueschists. **Sample 14-4B:** (a)  
571 Glaucophane + phengite + lawsonite layers alternated to discontinuous quartz-rich layers. Plane  
572 Polarized Light (PPL); (b) Glaucophane + phengite + lawsonite layer containing variably sized  
573 garnet Crosse Polarized Light (XPL); (c) Fine-grained idioblasts of lawsonite occur in  
574 association with glaucophane (PPL); **Sample 14-6F/G:** (d, e) Glaucophane with minor  
575 phengite defines the main foliation. The foliation is overgrown by lawsonite and garnet  
576 porphyroblasts (PPL); (f) Lawsonite porphyroblast is crosscut by thin quartz veins (XPL).

577

578 **Figure 3.** Representative photomicrographs of Type-I and Type-II fluid inclusions (PPL). (a)  
579 Type-I primary two-phase carbonic-aqueous inclusions in garnet (sample14-6F/G). (b) Type-I  
580 primary two-phase aqueous-carbonic inclusions in matrix quartz (sample 14-4B). (c) Type-IIa  
581 primary two-phase aqueous inclusions in quartz included in garnet (sample14-6F/G). (d) Type-  
582 IIb secondary two-phase aqueous inclusions and Type-III re-equilibrated inclusions in quartz  
583 (sample 14-4B).

584

585 **Figure 4.** Representative photomicrographs of Type-III fluid inclusions (PPL). (a) Re-  
586 equilibrated inclusions in quartz showing implosion textures (sample14-6F/G). (b) Re-  
587 equilibrated inclusions in quartz exhibiting necking and dendritic type networks of fluid  
588 inclusions (sample14-6F/G). (c) Re-equilibrated inclusion in quartz showing different  
589 morphologies: (i) hook-shape microstructure; (ii) “C” or “arc” shape, and (iii) necking and

590 stretched phenomena (sample 14-4B). **(d)** Dendritic type network of secondary fluid inclusions  
591 in quartz (sample 14-4B).

592

593 **Figure 5.** Histograms showing **(a)** homogenization temperature ( $T_h$ ), and **(b)** final melting  
594 temperature of  $\text{CO}_2$  for Type-I  $\text{CO}_2$ - $\text{H}_2\text{O}$  primary inclusions hosted in quartz and garnet.

595

596 **Figure 6.** Histograms showing final melting temperature of **(a)** Type-IIa primary  $\text{H}_2\text{O}$ - $\text{NaCl}$   
597 inclusions in quartz, and **(b)** Type-IIb secondary  $\text{H}_2\text{O}$ - $\text{NaCl}$  inclusions in quartz.

598

599 **Figure 7.** Histograms showing homogenization temperature ( $T_h$ ) for **(a)** Type-IIa primary  $\text{H}_2\text{O}$ -  
600  $\text{NaCl}$  inclusions in quartz, and **(b)** Type-IIb secondary  $\text{H}_2\text{O}$ - $\text{NaCl}$  inclusions in quartz.

601

602 **Figure 8.** Comparison between fluid inclusion isochores and the  $P$ - $T$  path (thick arrow in pink)  
603 recorded by blueschist from the Sapi-Shergol ophiolitic mélange (after Groppo et al., 2016).  
604 The lawsonite boundary is drawn after Zack et al. (2004). The yellow box shows peak  
605 metamorphic conditions. The retrograde path is mainly characterized by nearly isothermal  
606 decompression (as evident from hook shaped, annular inclusions and explosion type textures).  
607 The last portion of the  $P$ - $T$  path is characterized by isobaric cooling (as constrained by the  
608 development of dendritic type networks of inclusions).

609

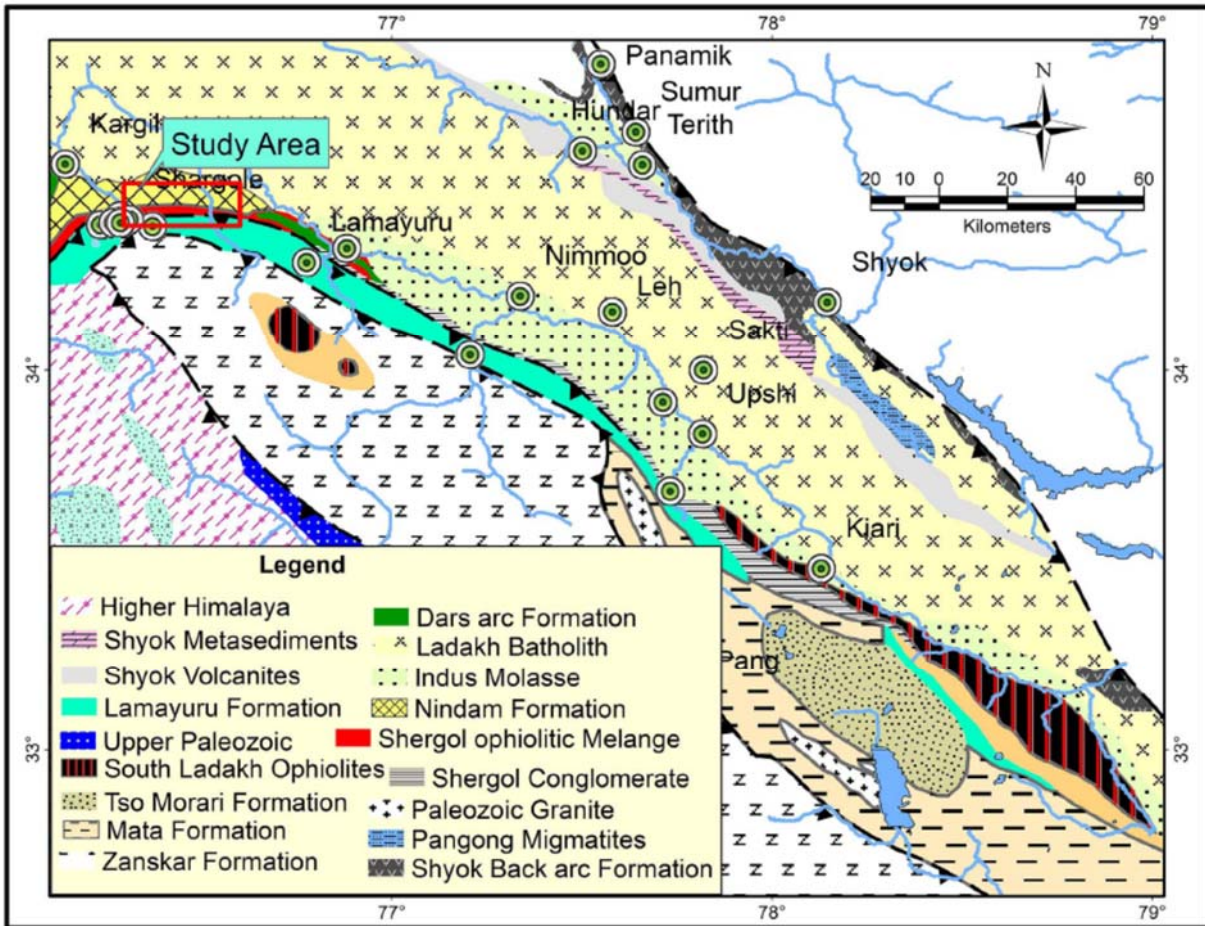
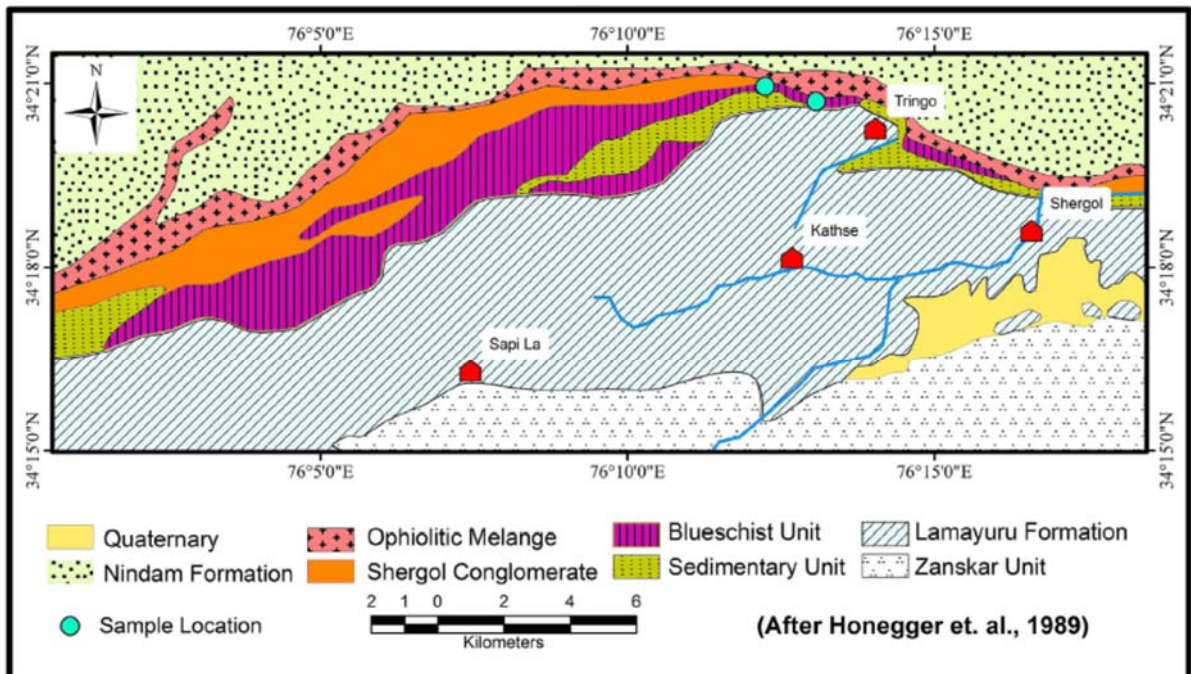


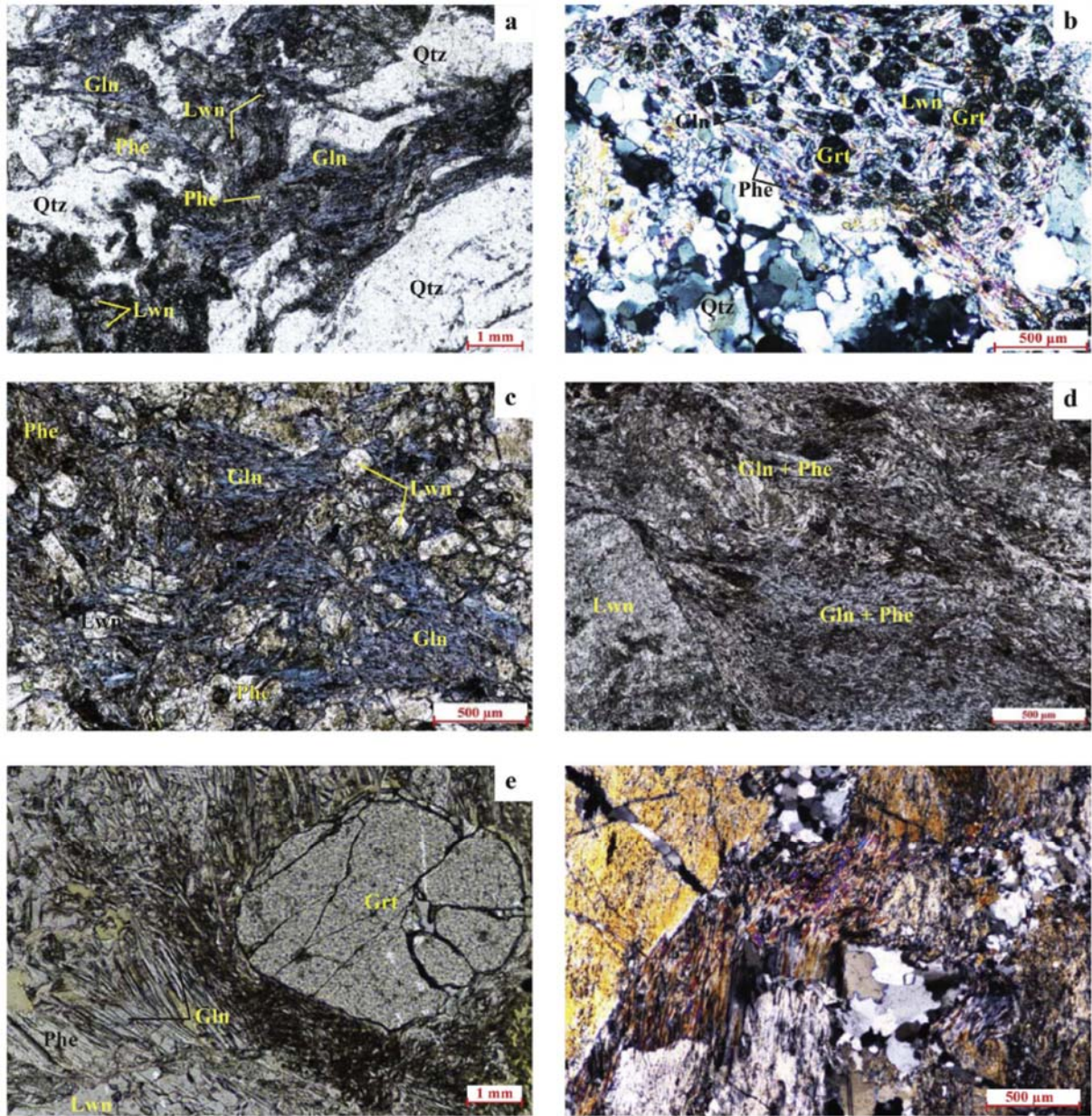
Fig. 1a



610

611 Fig. 1

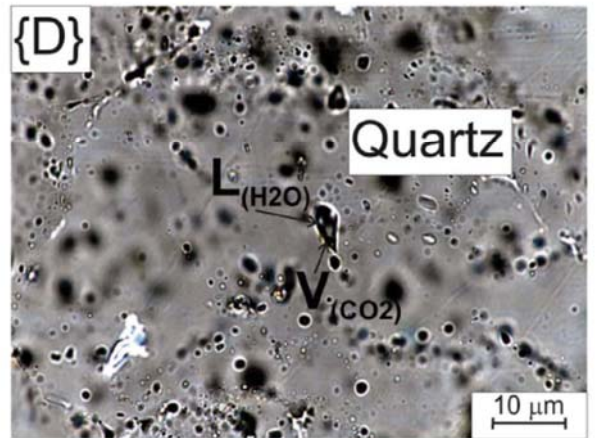
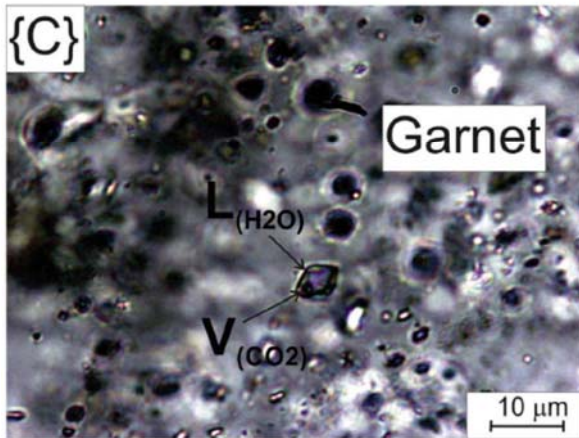
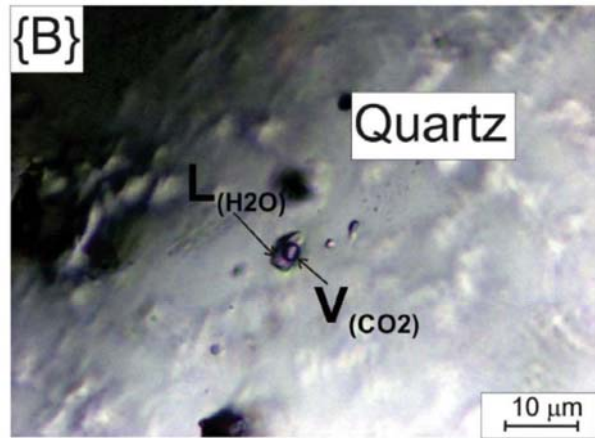
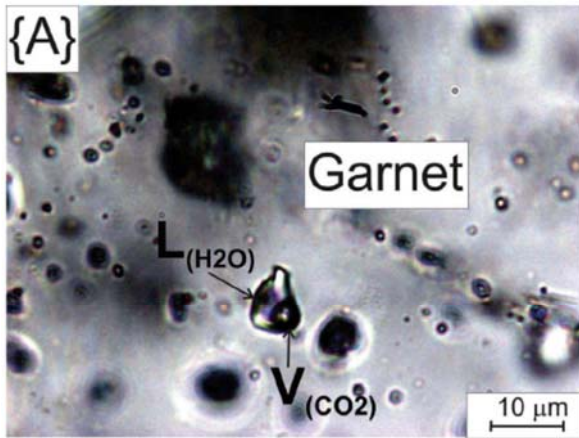
612



613

614 Fig. 2

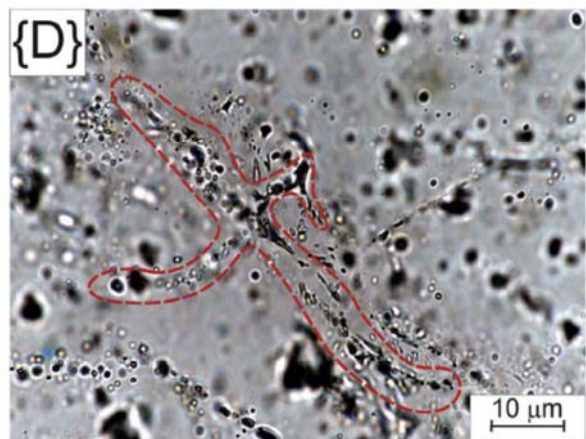
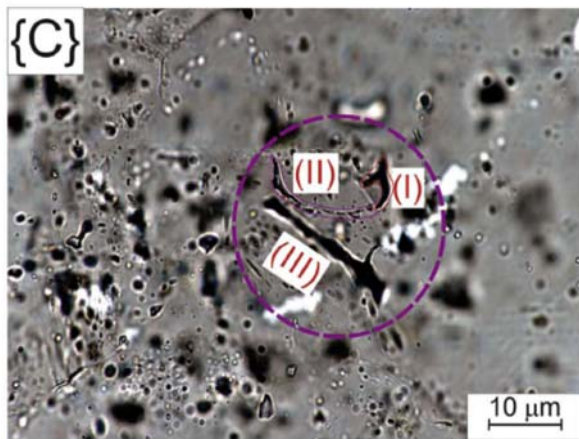
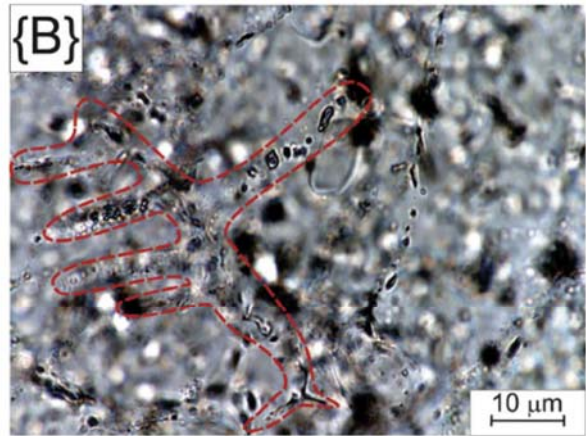
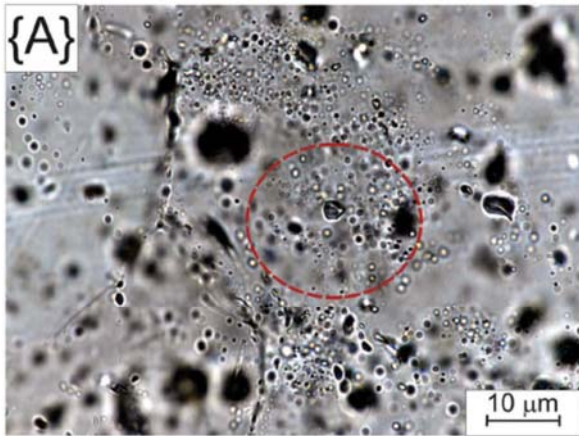
615



616

617 Fig. 3

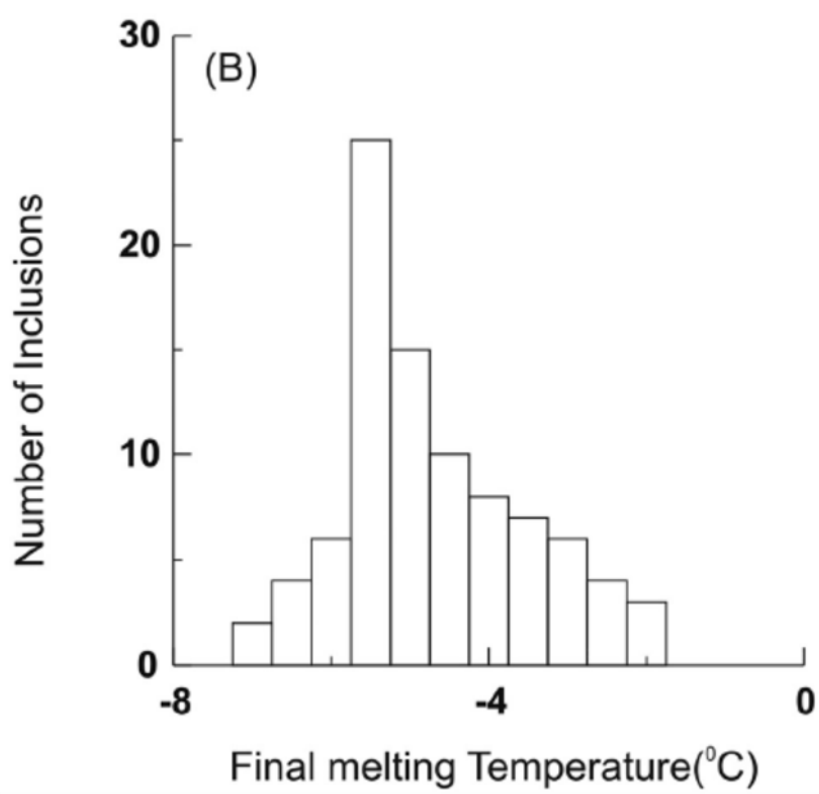
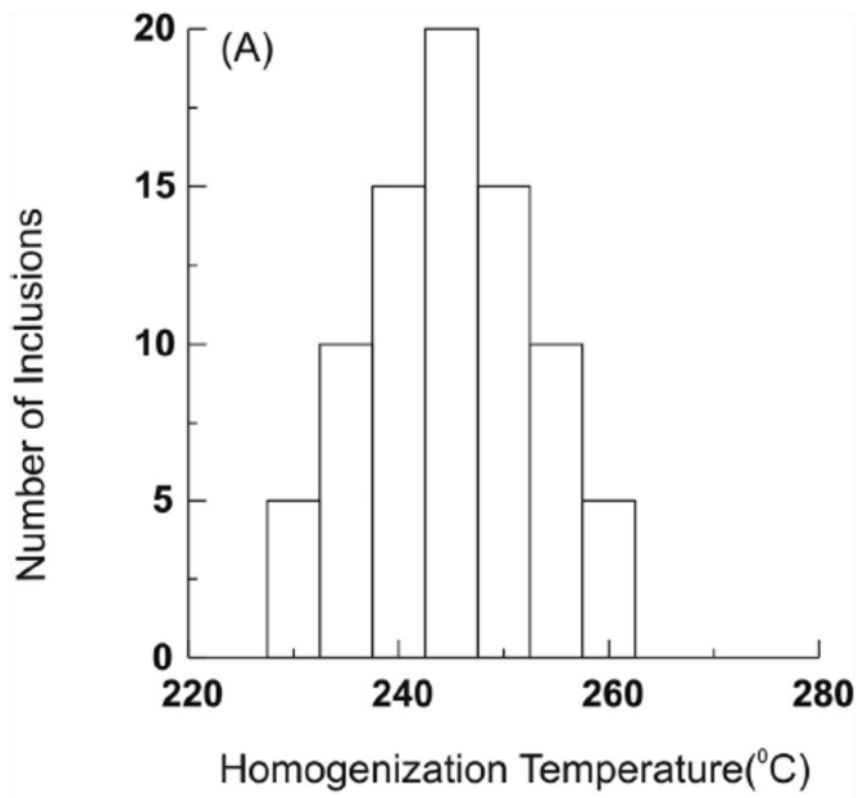
618



619

620 Fig. 4

621

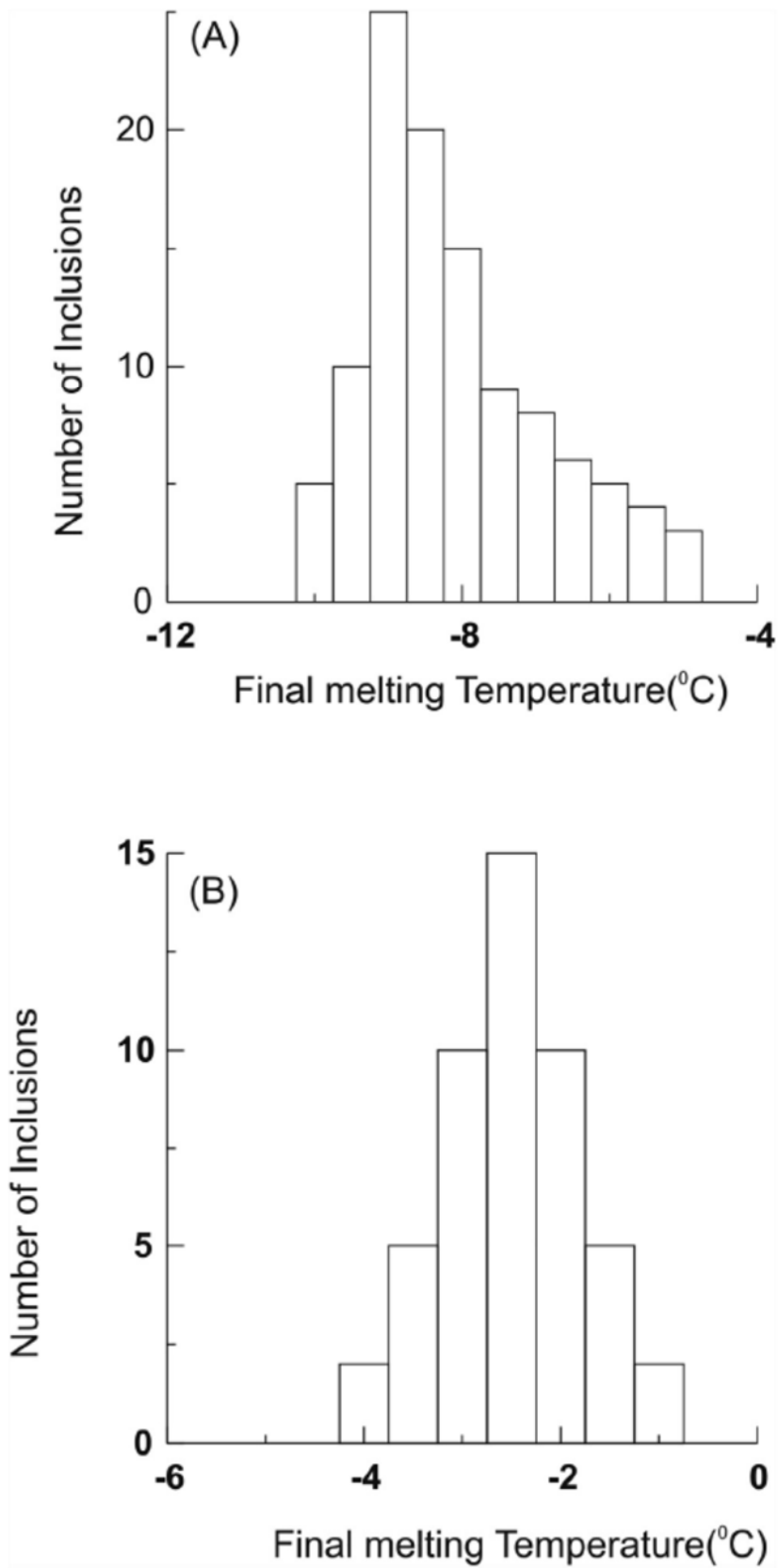


622

623 Fig. 5

624

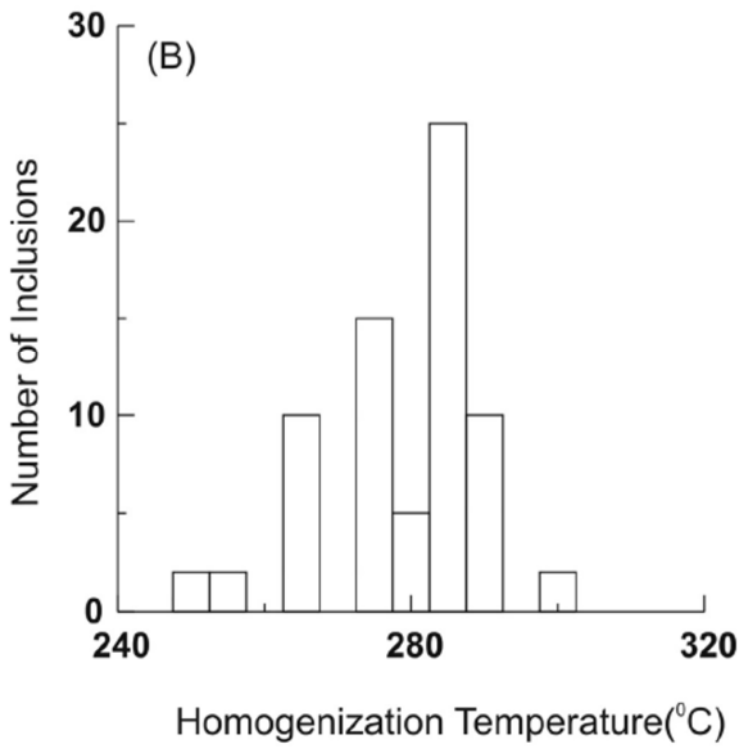
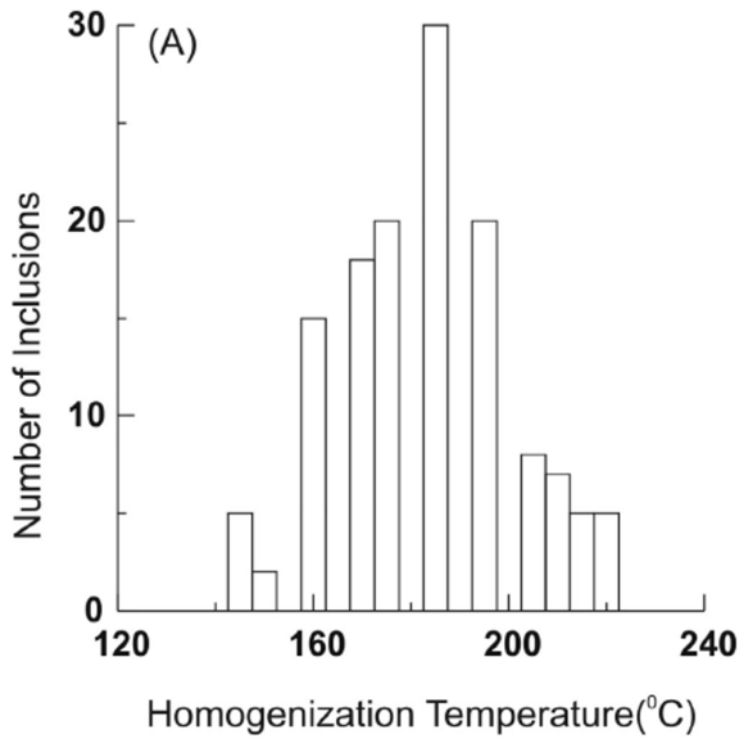




625

626 Fig. 6

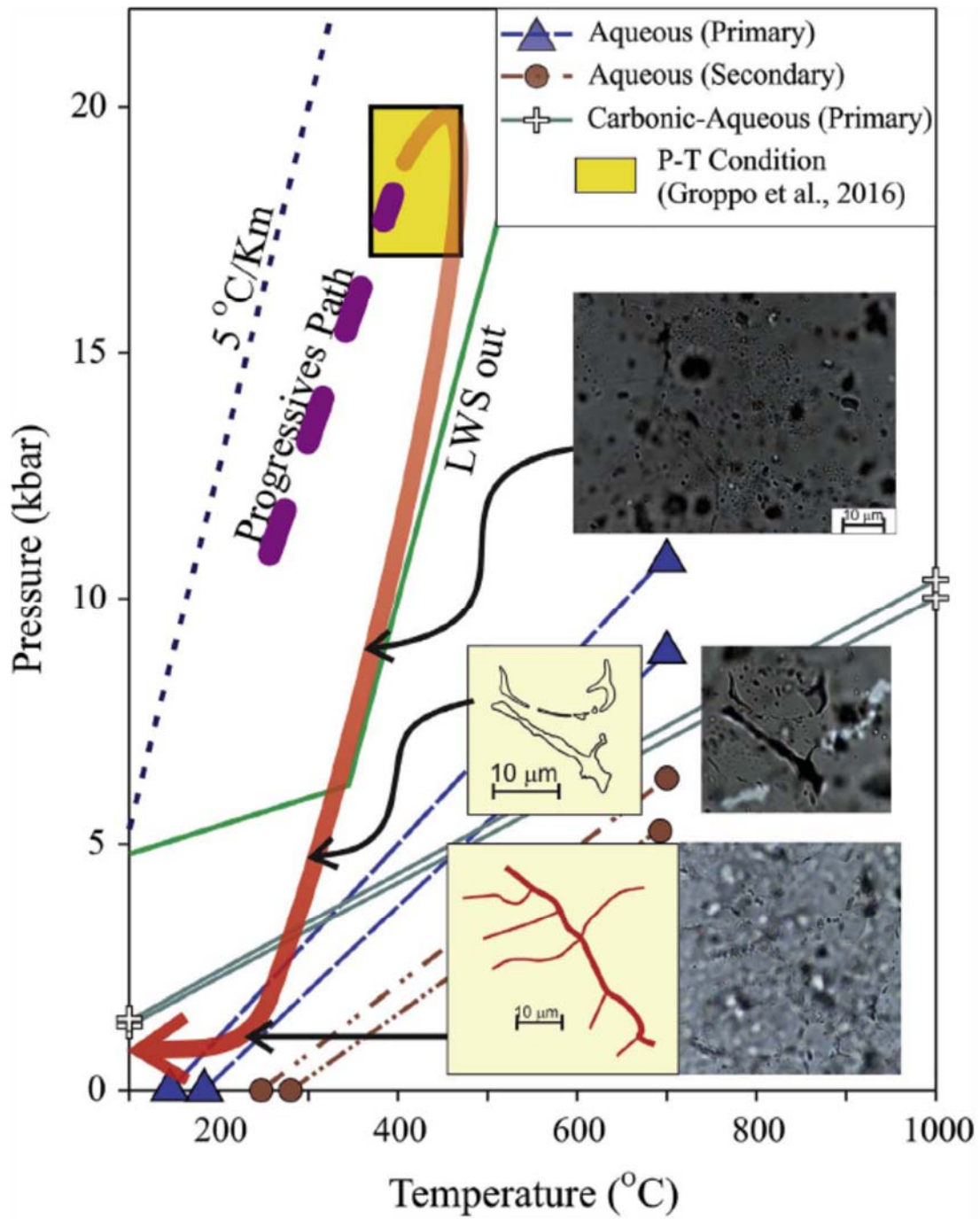
627



628

629 Fig- 7

630



631

632 Fig.8